Preprints.org

Article

Not peer-reviewed version

Topology Before Function: The Bauplan as the Structural Limit of Biological Execution

Tahir Rahman *

Posted Date: 13 April 2026

doi: 10.20944/preprints202604.0864.v1

Keywords: Bauplan; biological topology; ARCH × Φ model; gating mechanisms; extracellular matrix; Sonic hedgehog; YAP/TAZ; cardiac fibrosis

Preprints.org is a free multidisciplinary platform providing preprint service that is dedicated to making early versions of research outputs permanently available and citable. Preprints posted at Preprints.org appear in Web of Science, Crossref, Google Scholar, Scilit, Europe PMC.

Copyright: This open access article is published under a Creative Commons CC BY 4.0 license, which permit the free download, distribution, and reuse, provided that the author and preprint are cited in any reuse.

Preprints.org (www.preprints.org) | NOT PEER-REVIEWED | Posted: 13 April 2026 doi:10.20944/preprints202604.0864.v1

Disclaimer/Publisher's Note: The statements, opinions, and data contained in all publications are solely those of the individual author(s) and contributor(s) and not of MDPI and/or the editor(s). MDPI and/or the editor(s) disclaim responsibility for any injury to people or property resulting from any ideas, methods, instructions, or products referred to in the content.

Article

Topology Before Function: The Bauplan as the Structural Limit of Biological Execution

Tahir Rahman

Washington University in St. Louis, School of Medicine; trahman@wustl.edu

Abstract

Biological execution depends on the multiplicative convergence of four jointly necessary domains — Archetype (A), Drive (D), Context (C), and Gating Field (Φ) — as formalized in the ARCH × Φ framework. Prior applications of this framework treated the A-domain as a given structural substrate and focused primarily on sterol-dependent mechanisms underlying Φ. The present paper addresses this gap by proposing that the Bauplan — the conserved topological architecture of an organism's organs and appendages — is proposed as the physical instantiation of the A-domain. Bauplan is not a description of morphological outcome, but an upstream structural prerequisite that determines the ceiling of what any combination of D, C, and Φ can execute. We propose a four-tier hierarchy of A-domain constraint (phylotypic, ontogenetic, functional, and state), in which Tiers I–III define the Bauplan and Tier IV represents the configuration gated in real time by ARCH × Φ. Four lines of published empirical evidence are integrated. The fin-to-limb appendage system demonstrates conserved Bauplan specification via the ZRS enhancer across approximately 400 million years. Organ-level topology — including cardiac extracellular matrix architecture, hepatic lobular organization, and renal nephron geometry — shows that disruption of structural topology produces categorical execution failure independent of cellular viability. Minimal model systems, including the Caenorhabditis elegans connectome and the zebrafish Mauthner circuit, provide direct examples of Bauplan-as-circuit. Finally, pathological cardiac hypertrophy demonstrates that sustained Φ activation can drive partially irreversible Tier III A-domain remodeling through extracellular matrix fibrosis that persists after Φ normalization. We further propose that sterol derivatives may contribute to Φ regulation at both membrane and epigenetic levels. Oxysterols act as agonists of DNA methyltransferase 1, and steroid hormones activate nuclear receptor pathways that recruit chromatin-remodeling complexes, suggesting a potential linkage between membrane gating and chromatin state. Finally, we introduce Topological Connectivity Density (TCD), a metric derivable from second-harmonic generation microscopy of standard biopsy sections, as an operational measure of A-domain state. The framework predicts distinct failure modes in cirrhosis, dilated cardiomyopathy, and congenital malformations that are not reducible to D, C, or Φ deficits, but instead reflect irreversible disruption of underlying topological constraints.

Keywords: Bauplan; biological topology; ARCH × Φ model; gating mechanisms; extracellular matrix; Sonic hedgehog; YAP/TAZ; cardiac fibrosis

1. Introduction: What Determines What a Body Can Do?

1.1. The ARCH × Φ Framework

Biology's most fundamental question is not what a living system is, but what it does — and, more precisely, when it acts and when it does not. Threshold-governed execution events — the rattlesnake's eleven-millisecond strike, the Venus flytrap's snap, the clownfish's irreversible change from male to female — share a structural logic that single-variable accounts cannot explain. The ARCH × Φ framework formalizes this logic as a multiplicative threshold function:

© 2026 by the author(s). Distributed under a Creative Commons CC BY license.

Preprints.org (www.preprints.org) | NOT PEER-REVIEWED | Posted: 13 April 2026 doi:10.20944/preprints202604.0864.v1

$$R(t) = A \times D \times C \times \Phi(t) \geq \theta$$

where A (Archetype) is the conserved structural topology required for execution — the circuit, scaffold, or geometric template without which execution is physically impossible regardless of the other three domains. D (Drive) is the energetic or hormonal gradient that powers execution. C (Context) is the proximal triggering input that initiates the execution cascade. Φ (Gating Field) is the independently tunable permissiveness variable — sterol-modulated — that determines whether a fully charged, structurally intact, and contextually triggered system is allowed to act. (Rahman et al., 2025). The present paper concerns A specifically. The multiplicative structure predicts a zero-term veto: if any single domain approaches zero, the product R collapses regardless of the state of the remaining three.

The framework has begun validation in four published instantiations. Rahman et al. (2025) established the neuroevolutionary foundations, demonstrating that behavioral execution across five conserved systems (defense, mating, competition, caregiving, coalition) requires conjunctive alignment of all four domains. Rahman (2025) applied the framework to DNA replication initiation, mapping origin-licensing architecture to A, kinase and nucleotide drives to D, chromatin accessibility to C, and checkpoint-mediated phase control to Φ — predicting all-or-none S-phase entry and synergistic inhibition under multi-domain partial reduction. Rahman (2026a) applied the framework to clownfish sex change, where male-to-female transition requires structural gonadal readiness (A), estrogenic endocrine bias (D), dominant female removal (C), and developmental gating (Φ) — with partial domain alignment producing metastable intermediate states and sustained alignment above threshold yielding irreversible commitment with hysteresis. Rahman (2026b) applied the framework to Venus flytrap closure, where bistable snap-buckle geometry (A), H^+-ATPase electrochemical drive (D), temporally paired trigger-hair signals (C), and phytosterol-dependent membrane excitability (Φ) must jointly exceed threshold — the C-domain temporal requirement demonstrating zero-term veto in a plant without a nervous system. Multiple lines of evidence suggest that the physical origin of Φ lies in sterol incorporation into eukaryotic membranes during the Great Oxidation Event, when oxygen-dependent sterol biosynthesis and sterane biomarkers first appear in the rock record, and when sterols become defining components of eukaryotic membranes. Sterols dramatically alter membrane dynamics and gating of ion channels and transporters, providing a natural substrate for a tunable permissiveness field (Jiang, 2019).

1.2. The A-Domain Gap

All four published instantiations treat A as a given: origin-licensing machinery exists; gonadal architecture is present; snap-buckle geometry is intact; neural circuits are wired. What determines these A-domain structures? What makes the rattlesnake's strike circuit different from the tortoise's? Why is the human hand topologically identical — five digits, proximal-to-distal HoxA/D gradient, posterior Sonic hedgehog signaling — to a bat wing, a horse hoof, and a whale flipper, despite radically different sizes, shapes, and functions? And why does cirrhosis abolish hepatic metabolic zonation even when abundant viable hepatocytes remain?

These questions share a single answer: the Bauplan. The conserved topological architecture of organs and appendages is not merely a developmental outcome but a structural constraint — the upstream prerequisite that determines the ceiling of what any combination of D, C, and Φ can execute. The present paper makes this argument explicit, defines the Bauplan as the A-domain of the ARCH × Φ framework, provides four empirical lines of evidence, and proposes a quantitative metric (Topological Connectivity Density, TCD) that allows A-domain state to be measured from standard biopsy material.

© 2026 by the author(s). Distributed under a Creative Commons CC BY license.

Preprints.org (www.preprints.org) | NOT PEER-REVIEWED | Posted: 13 April 2026 doi:10.20944/preprints202604.0864.v1

1.3. Three Empirical Anchors and a Formal Claim

The argument proceeds in three empirical registers and one formal claim. The formal claim is: A is topology, not metricity. A whale flipper and a human hand share the same topological A (proximal-to-distal axis, five-digit HoxD specification, posterior Shh ZPA); their D, C, and Φ produce radically different metrical outputs (size and shape) within that topological constraint. This distinction resolves a persistent confusion: growth-regulation models (Hippo/YAP-TAZ, mTOR) explain metrical outcomes but do not explain what sets the topological template. This topology/metricity distinction has an independent formal analog in the morphometrics literature, where allometry (scaling relationships between organ sizes) and geometric morphometrics (spatial configuration of homologous landmarks independent of size) are recognized as partially separable descriptors of biological form (Cobham & Mirth, 2020). The present framework extends this distinction from population-level statistical description to developmental mechanism: topology functions as an upstream structural prerequisite, not merely a different measurement of the same phenomenon. The Bauplan-as-A framework supplies that explanation.

The three empirical registers are: (1) appendage evolution, providing the purest molecular evidence for conserved A-domain specification across 400 million years; (2) organ architecture, providing clinical and experimental evidence that topological Bauplan disruption produces execution failure that no plausible combination of D, C, or Φ appears sufficient to compensate; and (3) minimal model systems, providing the most direct demonstrations of zero-term veto from Bauplan ablation.

$$R = A \cdot D \cdot C \cdot \Phi \geq \theta$$

R	Execution output
A	Structural topology — conserved architecture of the executing system; time-invariant under physiological conditions
D	Drive — electrochemical or biochemical energy gradient (ATP, CDK activity, hemodynamic load)
C	Context — triggering input, regardless of modality
Φ	Gating field — sterol-modulated membrane permissiveness
θ	System-specific commitment threshold

Suppression of any single term drives R → 0 regardless of the others (zero-term veto). A is the only time-invariant term: loss of D, C, or Φ is potentially reversible; loss of A is not.

2. What the ARCH × Φ Framework Is: Three Instantiations

2.1. DNA Replication: A Molecular Zero-Term Veto

DNA replication provides the clearest molecular demonstration of the ARCH × Φ architecture because its four domains are biochemically distinct, independently manipulable, and all required (Rahman, 2025). A is the origin-licensing architecture: the ORC-MCM replication machinery assembled at replication origins, determining where and how many initiation events are geometrically possible. D is the integrated metabolic and kinase drive: CDK activity, dNTP pools, and ATP-dependent helicase loading. C is chromatin accessibility: the epigenetic state of origin-adjacent chromatin that determines whether the licensing machinery can engage. Φ is checkpoint-mediated phase control: the cell-cycle gating mechanism, operationalized as Rb-E2F bistability and

© 2026 by the author(s). Distributed under a Creative Commons CC BY license.

Preprints.org (www.preprints.org) | NOT PEER-REVIEWED | Posted: 13 April 2026 doi:10.20944/preprints202604.0864.v1

ATM/ATR checkpoint kinase activity, that gates whether a fully licensed, energetically charged, accessible origin is actually permitted to fire.

The zero-term veto is observed in four distinct configurations. Checkpoint activation ($\Phi \to 0$) arrests S-phase entry despite intact origin architecture, adequate dNTPs, and permissive chromatin — this is an example of the molecular Φ veto. Origin deletion ($A \to 0$ locally) eliminates replication from that region regardless of how much CDK is active or how open the chromatin is — the structural veto. Nucleotide depletion ($D \to 0$) prevents fork progression despite intact licensing and open chromatin. And heterochromatin at origin-adjacent regions ($C \to 0$) prevents licensing regardless of kinase activity or checkpoint state. All four are experimentally documented single-domain zero-term vetoes (Bell and Dutta, 2002; Barr et al., 2016). Critically, the multiplicative structure predicts that combining 50% reduction in two domains produces ≥75% suppression of replication initiation — not ~50% as additive models predict — a falsifiable distinction (Rahman, 2025).

2.2. Clownfish Sex Change: Hysteresis and Irreversibility

Socially controlled sex change in *Amphiprion* spp. provides the most biologically accessible demonstration of ARCH × Φ's prediction that partial domain alignment produces metastable intermediate states and that sustained alignment above threshold produces irreversible commitment with hysteresis (Rahman, 2026a). A is the latent structural readiness of gonadal and neural substrates: the bipotential gonad present in all clownfish retaining both ovarian and testicular tissue, the preoptic area circuit topology that can support either male or female behavioral programs (Parker et al., 2024). D is estrogenic endocrine bias: the aromatase expression shift from male-typical to female-typical, mediated by the CYP19a1a locus in both brain and gonad (Casas et al., 2016). C is social permissiveness: the removal of the dominant female, which is the specific releasing trigger that initiates the transition cascade. Φ is developmental and temporal gating: the chromatin state and steroid hormone milieu that determine whether the gonadal commitment program can be executed.

The ARCH × Φ prediction that partial domain alignment stabilizes intermediate states without commitment is directly supported: sex-changing fish exhibit a stable, male-like behavioral phenotype that persists throughout the transition until gonadal sex change is complete, rather than showing progressive feminization (Parker et al., 2022). This is not a simple intermediate along a continuum — it is a metastable state in which A, D, and C are partially aligned but Φ has not crossed the commitment threshold. The irreversibility of full commitment, once threshold is exceeded, reflects strong Φ-level hysteresis: the forward threshold (male to female) is substantially lower than the reverse threshold (female to male), producing a bistable system with unequal commitment barriers. This asymmetry is precisely what the Φ-reversibility principle predicts: execution events whose reversal carries high fitness cost exhibit strong hysteresis in Φ dynamics.

2.3. Venus Flytrap: Zero-Term Veto Without a Nervous System

The Venus flytrap (*Dionaea muscipula*) is the most important ARCH × Φ instantiation for the present paper because it demonstrates the zero-term veto in a system without neurons, providing the strongest available evidence that the multiplicative threshold architecture is a general property of biological execution rather than a product of nervous system organization (Rahman, 2026b).

A is the bistable snap-buckle trap geometry: the mechanical architecture of the lobes, midrib, and trigger hairs that enables rapid snap-closure when a critical curvature threshold is crossed. This geometry is the structural prerequisite — a flat leaf cannot perform trap closure regardless of H^+-ATPase drive or trigger-hair signal. D is the H^+-ATPase electrochemical drive maintaining the resting membrane potential (approximately −120 mV, substantially more negative than animal neurons) and the proton motive force that powers rapid ion flux during closure. C is the temporally paired trigger-hair signal: two action potentials within a ~20-second window, encoding the presence of struggling prey rather than a single environmental perturbation such as a raindrop. Φ is phytosterol-dependent membrane excitability: the plasma membrane lipid composition that determines the threshold for

© 2026 by the author(s). Distributed under a Creative Commons CC BY license.

Preprints.org (www.preprints.org) | NOT PEER-REVIEWED | Posted: 13 April 2026 doi:10.20944/preprints202604.0864.v1

action potential initiation. Phytosterol depletion raises the action potential threshold, reducing C-domain efficacy at any given stimulus intensity (Hedrich et al., 2016).

The C-domain temporal requirement is the clearest zero-term veto demonstration in any system. A single trigger-hair deflection, regardless of force or duration, cannot produce trap closure — the first action potential simply dissipates without commitment. Only the second deflection within the permissive window sums with the residual electrical memory of the first to exceed threshold. This is a C-domain zero-term veto: the structural machinery is intact (A), the electrochemical drive is fully charged (D), the membrane is permissive (Φ), but the temporal conjunction in C is not met and R = 0. No amount of increased drive, no manipulated phytosterol state, and no alteration of snap-buckle geometry can substitute for the C-domain temporal conjunction (Böhm et al., 2016).

3. Redefining A, D, C, and Φ for Organ Morphology

3.1. Archetype and Topology

The translation of the ARCH × Φ framework from behavioral and cellular contexts to organ morphology requires careful re-examination of what each domain means when the system in question is an organ maintaining its shape, size, and functional architecture over a lifetime. The central theory is that the A-domain at the organ level is topological rather than metrical. A whale flipper and a human hand share A. A healthy liver and a regenerating liver after partial hepatectomy share A. A normal heart and an athlete's physiologically hypertrophied heart share A. What distinguishes them is D × C × Φ operating within the topological constraint A sets. Cirrhosis does not reduce A — it destroys it. That is why hepatocytes in a cirrhotic liver cannot reconstitute metabolic zonation even when their cell-intrinsic machinery is intact.

3.2. A — ECM Scaffold Topology and Circuit Geometry

At the organ level, A is the extracellular matrix scaffold topology plus the topological connectivity of the organ's functional circuit. For the heart, this means the three-dimensional collagen network architecture, the chamber geometry established by regional ECM expansion during morphogenesis, and the conduction system wiring (SA node → AV node → bundle of His → Purkinje fibers). For the liver, it is the hexagonal lobular architecture — central vein at the geometric center, portal triads at the six vertices, sinusoidal connections at a specific diffusion distance — that encodes both the metabolic zonation gradient and the regenerative template. For the kidney, it is the hairpin geometry of the loop of Henle, which is the mechanistic prerequisite for countercurrent multiplication.

The key finding from decellularization experiments — removing all cells from an organ while preserving its ECM — directly answers whether A is cell-encoded or scaffold-encoded. When human liver tissue is completely decellularized, the lobular hexagonal topology persists: portal tracts remain in their characteristic positions, sinusoidal network architecture is maintained, and the scaffold retains the positional identity cues that direct reseeded hepatocytes to adopt zone-specific gene expression programs (Mazza et al., 2015; Baptista et al., 2011). The Bauplan is etched into the permanent ECM scaffold, not carried by the cells. Cells maintain and dynamically regulate Tier III A (functional configuration), but Tier I–II topology (phylotypic and ontogenetic Bauplan) is scaffolded. This may be why cirrhosis — which replaces the lobular scaffold with fibrous septa — abolishes zonation even with abundant viable hepatocytes. The independence of topological template from metrical output is further demonstrated in the Drosophila wing-haltere system: the Hox gene Ultrabithorax reduces Dpp morphogen concentration and spread in the haltere relative to the wing, producing organs with identical topological identity but approximately 3.5–4-fold different sizes (Cobham & Mirth, 2020; Weatherbee et al., 1998). Metrical output is modulated by D-domain signals operating within an invariant A-domain topological template — the Bauplan is shared; the execution output differs.

© 2026 by the author(s). Distributed under a Creative Commons CC BY license.

Preprints.org (www.preprints.org) | NOT PEER-REVIEWED | Posted: 13 April 2026 doi:10.20944/preprints202604.0864.v1

The cardiac ECM makes the same argument with equal clarity. Acute disruption of the fibrillar collagen network decreases myocardial systolic performance without changing myocyte contractility (Baicu et al., 2003). The ECM is not a passive scaffold — it physically couples cardiomyocyte contraction to chamber mechanics through the collagen network, transmits force through the ventricular wall, and maintains the spatial organization of gap junctions that ensures conduction continuity. Destroy A while leaving D, C, and Φ intact and execution fails.

3.3. D — Metabolic-Hemodynamic Demand

Drive at the organ level is the integrated demand signal the organ continuously receives from the body. For the heart, D is wall stress and cardiac output demand, transmitted through mechanosensitive pathways including integrins, stretch-activated channels, and the Piezo1 mechanosensor. For the liver, D is portal blood flow and pressure — the hemodynamic signal that simultaneously initiates regeneration after partial hepatectomy and, when restored to normal by adequate liver mass, terminates it. Portal pressure doubles after 70% hepatectomy in mice, and this surge in portal shear stress activates Piezo1 on liver sinusoidal endothelial cells, which releases paracrine hepatocyte growth factor to initiate hepatocyte proliferation (Miyaoka et al., 2012).

This definition of D as demand rather than stored potential resolves a feature of organ biology that additive models cannot explain: why organs size to functional demand. D is the demand itself, and D drives growth execution when combined with adequate A, C, and Φ. When D is restored to normal (by sufficient mass after regeneration, or by mechanical unloading after pressure overload), growth terminates — not because some fixed program runs out, but because the D-domain signal that combined with the other domains to exceed θ has normalized.

3.4. C — The Releasing Trigger

Context at the organ level is the specific signal that initiates a discrete execution event. For liver regeneration, C is the portal hemodynamic surge after hepatectomy — an acute mechanical trigger distinguishable from the chronic background D. For cardiac hypertrophy, C is pressure overload above a threshold wall stress. For organ morphogenesis during development, C is the positional signal — retinoic acid gradient, FGF from the apical ectodermal ridge, Sonic hedgehog from the notochord — that specifies where and when a particular execution program is licensed. Crucially, C for the developing heart tube is the organ's own hemodynamic output: the heart shapes itself partly in response to the flow it generates, making C a self-referential signal in early morphogenesis (Christoffels and Moorman, 2009). This is not unusual in the ARCH framework — in the clownfish, C (dominant female removal) is partly constituted by the animal's own behavioral repertoire.

3.5. Φ — YAP/TAZ, Chromatin State, and the Sterol Connection

Φ at the organ level operates at two tiers that correspond precisely to the membrane and epigenetic tiers described in the companion paper (Rahman and Zorumski, in preparation).

At the acute-to-intermediate timescale, Φ is YAP/TAZ nuclear permissiveness, gated by the Hippo kinase cascade. When Hippo is active — responding to cell-cell contact, apicobasal polarity, and ECM mechanics — LATS1/2 phosphorylates YAP/TAZ, sequestering them in the cytoplasm and vetoing growth execution regardless of the state of D, C, and A (Piccolo et al., 2014; Zanconato et al., 2016). When Hippo is inactive, YAP/TAZ enter the nucleus and gate proliferation and organ growth. This gating function is confirmed by the compartment-specific dAkt experiments in Drosophila: selective reduction of insulin pathway activity in the posterior wing compartment produces a small but correctly patterned compartment, while the adjacent anterior compartment is entirely unaffected in size and patterning (Hafen & Stocker, 2003). Size-control pathways — whether insulin/PI3K or Hippo/YAP-TAZ — modulate metrical output within an intact topological template; neither pathway specifies or alters the template itself (Yang & Xu, 2011). This is Φ in the strict ARCH sense: independent of D (it is not activated simply by high metabolic demand), independently tunable from

© 2026 by the author(s). Distributed under a Creative Commons CC BY license.

Preprints.org (www.preprints.org) | NOT PEER-REVIEWED | Posted: 13 April 2026 doi:10.20944/preprints202604.0864.v1

A (ECM mechanics activate YAP/TAZ by reading the stiffness of the A-domain scaffold, but the two remain separable), and capable of zero-term veto. Critically, YAP/TAZ is a Φ gate that reads out A (ECM mechanics) and D, but its overactivation alters cell number and wall thickness without inventing new circuits or lobular topologies. This marks a distinction between Φ and A.

At the lifetime timescale, Φ is chromatin state: the HDAC/HAT balance and DNA methylation landscape that determines which gene programs are accessible. In cardiac hypertrophy, pressure-overload stress reactivates Brg1, the ATPase subunit of the BAF chromatin-remodeling complex, which forms a ternary complex with HDAC and PARP to execute the α-MHC to β-MHC isoform switch — a return to the fetal gene program (Hang et al., 2010). This is Φ operating at the epigenetic tier: HDAC inhibitors block this switch and attenuate hypertrophic growth in a dose-dependent fashion (Antos et al., 2003; Kee et al., 2006). The histone modifications at both MHC loci normalize when the Brg1-HDAC complex is disbanded, confirming reversibility at this tier (Hang et al., 2010).

3.6. Are Sterols Involved in Epigenetic Φ?

Sterols are well-established molecular substrates for membrane excitability and signaling, and this section examines whether they are also involved in epigenetic Φ. Oxysterols act as direct agonists of DNA methyltransferase 1 (DNMT1). At elevated concentrations, 25-hydroxycholesterol (25-HC) promotes methylation of CpG islands as an endogenous agonist of DNMT1, regulating transcription of voltage-gated calcium channel subunits, calcium-calmodulin kinases, and genes involved in lipid metabolism and MAPK signaling (Wang et al., 2020; Meaney, 2014). This places oxysterols — which are rapid-timescale Tier 1 Φ modulators at the membrane level — also in the epigenetic tier, where they shape the chromatin landscape on hours-to-days timescales. Steroid hormones operate through nuclear hormone receptors (NHRs) — LXR, FXR, PXR, CAR, RXR — which are activated by oxysterols, bile acids, and steroid hormone derivatives (Motola et al., 2006). Ligand binding to these receptors recruits HAT complexes (p300, ASCOM) that acetylate histones at target promoters, and chromatin-remodeling complexes including BRG1 and BAF that remodel chromatin accessibility (Kemper et al., 2009). This means that steroid hormones — which are Tier 2 Φ modulators in the neurosteroid framework — also directly regulate the epigenetic Φ landscape through NHR-mediated chromatin remodeling.

The mevalonate pathway, which produces cholesterol as its end product, is regulated by BET bromodomain epigenetic readers: inhibition of BET proteins reduces intracellular cholesterol levels by regulating genes involved in cholesterol biosynthesis, uptake, and intracellular trafficking (Gilham et al., 2022). This creates a bidirectional feedback: cholesterol metabolites (oxysterols, steroids) regulate epigenetic marks, and epigenetic readers (BET proteins) regulate cholesterol synthesis. Sterols are therefore not merely the molecular substrate of membrane Φ; they are integrated into epigenetic Φ at multiple levels — as DNMT1 agonists, as NHR ligands that recruit chromatin-remodeling complexes, and as downstream products of BET-regulated biosynthesis.

This establishes sterols as the molecule that operates all three tiers of Φ simultaneously: Tier 1 (membrane dipole potential and ion channel gating via cholesterol and oxysterols), Tier 2 (neurosteroid GABA-A receptor modulation via allopregnanolone and related compounds), and Tier 3 (epigenetic chromatin state via oxysterol-DNMT1 and steroid hormone-NHR-HAT cascades). No other known molecular class spans all three. This convergence is not coincidental — it reflects the evolutionary depth of sterol-based regulation, which predates the separation of behavioral, cellular, and organ-level ARCH × Φ instantiations.

3.7. Cellular Bauplan: Intracellular Topology as the A-Domain

At the cellular scale, the same principle holds: the A-domain is not reducible to molecular inventory, but depends on intracellular topology. The execution capacity of a cell is determined by the spatial organization of its structural components — the cytoskeletal tensegrity architecture, nuclear lamina organization, and apicobasal polarity axis — which together constitute a cellular Bauplan.

© 2026 by the author(s). Distributed under a Creative Commons CC BY license.

Preprints.org (www.preprints.org) | NOT PEER-REVIEWED | Posted: 13 April 2026 doi:10.20944/preprints202604.0864.v1

This distinction mirrors the topology/metricity separation observed at the organ level. Altering protein concentration or kinase activity modulates execution amplitude, but does not change which execution events are geometrically possible. By contrast, altering topology — for example, disrupting spindle bipolarity or nuclear lamina organization — produces categorical execution failure despite intact energetic drive, signaling context, and checkpoint permissiveness.

Laminopathies provide a direct illustration. Mutations in LMNA disrupt nuclear lamina topology, reorganizing chromatin domains and replication timing architecture. The consequence is not a reduction in replication rate but a failure of replication program execution itself, despite intact CDK activity, chromatin accessibility, and checkpoint signaling. This is the cellular analog of Bauplan disruption at the organ level: topology loss produces execution failure that downstream domains cannot compensate.

These observations suggest that organ-level Bauplan is itself an emergent property of cellular Bauplan. The extracellular matrix scaffold and circuit geometries that define organ A-domain topology are constructed by cells operating under their own intracellular topological constraints. The A-domain is therefore recursively defined across scales, from intracellular architecture to organ morphology.

4. Empirical Proof Line 1: Deep Homology and the Appendage Bauplan

4.1. The ZRS Enhancer: Bauplan Encoded in 770 Base Pairs

The zone of polarizing activity regulatory sequence (ZRS) is a single 770 bp cis-regulatory element, located approximately 1 megabase from the Shh promoter within intron 5 of the Lmbr1 gene, that is solely responsible for Sonic hedgehog expression in the vertebrate limb and fin ZPA (Lettice et al., 2003; Sagai et al., 2005). This enhancer is the molecular specification of the topological Bauplan for the appendage: it encodes which cells express Shh, defining the posterior margin that organizes the anterior-posterior axis, digit identity, and digit number.

The conservation of this enhancer is remarkable. The mouse ZRS shares more than 70% sequence identity with the coelacanth ortholog across 400 million years of evolution, despite the enormous morphological changes separating fish fins from mammalian limbs (Lettice et al., 2017). When the coelacanth ZRS is transplanted into a mouse transgenic assay, it drives Shh expression in the correct ZPA domain and supports normal limb development despite sharing only 57% sequence similarity with the human ortholog, less than the python ZRS which fails (Kvon et al., 2016). The A-domain topological program is functionally interchangeable across 400 million years of evolution. The fish enhancer makes mammalian limbs.

The ZRS is therefore the most compelling available evidence that Bauplan is encoded in conserved cis-regulatory elements — the molecular grammar that specifies A — and that this grammar is conserved across evolutionary time independently of the metrical outputs (size and shape) it produces.

4.2. Paddlefish: Bauplan Predates the Structure It Specifies

If Bauplan is the A-domain prerequisite for an execution event, one prediction is that the Bauplan molecular program should be detectable before the structure it specifies appears in evolution. The paddlefish experiment confirms this prediction with exceptional clarity. Analysis of HoxA and HoxD gene expression in the developing pectoral fin of paddlefish (Polyodon spathula) — a basal actinopterygian that has never had digits — reveals the two-phase Hox expression pattern long considered a unique developmental signature of the tetrapod autopod (wrist and digits) (Davis et al., 2007; Shubin et al., 2009). The molecular A-domain program for digit topology predates digits by hundreds of millions of years.

As Shubin noted following this discovery: the capability to build limbs with fingers and toes existed for a long period of time, but it took a set of environmental triggers — a novel ecological context (C in the ARCH framework) — to make use of that capability (Davis et al., 2007). This

© 2026 by the author(s). Distributed under a Creative Commons CC BY license.

Preprints.org (www.preprints.org) | NOT PEER-REVIEWED | Posted: 13 April 2026 doi:10.20944/preprints202604.0864.v1

precisely maps onto the ARCH architecture: A (the HoxD Bauplan program) predated the execution event it now specifies; C (Late Devonian shallow-stream ecology) provided the releasing trigger; D and Φ supplied drive and permissiveness. The A-domain molecular grammar was waiting.

4.3. The Snake Series: A → 0 from Bauplan Erosion Across Evolutionary Time

The snake limblessness data provides the most powerful available demonstration that A-domain failure produces categorical execution veto regardless of the state of D, C, and Φ — and does so in an evolutionary series that shows the transition from partial A to zero A in precise molecular and morphological detail.

Basal snakes (pythons, boas) retain a partially degraded ZRS in which specific transcription factor binding sites have been lost through point mutations and deletions. The functional consequence is precisely what the ARCH framework predicts: partial A produces partial, abortive execution. Python embryos initiate hindlimb development — pre-chondrogenic condensations of tibia, fibula, and footplate form during early development — but the HOXD gene programs then drive toward a transient autopodial (digit) domain that dissolves within 24 hours of oviposition because the ZRS-Shh circuit that would sustain limb outgrowth is insufficient (Leal and Cohn, 2016). D is intact (metabolic machinery present), C is intact (positional developmental signals present), and Φ is intact (HOXD digit enhancers conserved in pythons) — but partial A produces partial execution that cannot be maintained.

Advanced snakes (vipers, rattlesnakes, cobras, corn snakes) have fully degraded ZRS sequences and produce no limb structures whatsoever. Genomic enhancer replacement experiments — inserting the python ZRS into a mouse genome in place of the normal mouse ZRS — cause severe limb reduction, confirming that ZRS degradation is causally sufficient for limb failure even in a background with intact D, C, and Φ machinery (Kvon et al., 2016). Single-nucleotide reversion of a key degraded transcription factor binding site in the ZRS is sufficient to rescue normal limb enhancer activity in mouse transgenic assays (Kvon et al., 2016), demonstrating the dose-sensitivity of A-domain specification.

Polydactyly data from ZRS point mutations extends this argument: single nucleotide changes at more than 20 distinct positions across the ZRS cause preaxial polydactyly — qualitative Bauplan topology changes producing extra or ectopic digits, not merely quantitative changes in limb size (Lettice et al., 2003, 2008; Lettice et al., 2017). The A-domain is not binary; it is a precisely specified topological grammar whose perturbation produces qualitatively distinct structural outputs that the ARCH framework predicts as partial A producing partial execution — in this case, an aberrant Bauplan rather than no Bauplan.

5. Empirical Proof Line 2: Organ Topology as Bauplan

5.1. The Heart: ECM Scaffold and the Conduction System Bauplan

The cardiac ECM is not a passive filler. It is a three-dimensional network of collagens, glycosaminoglycans, and glycoproteins that provides mechanical continuity between cardiomyocytes, transmits forces across the ventricular wall, maintains the spatial organization of gap junctions, and — during development — provides the morphogenetic signals that pattern chamber topology. Critically, regionalized ECM expansion drives chamber shape: CRISPR-Cas9 deletion of Hapln1a in zebrafish, which disrupts asymmetric cardiac ECM crosslinking, reduces atrial size and impairs chamber ballooning despite intact myocardial cell number, signaling, and contractility (Derrick et al., 2022). The ECM scaffold topology determines whether the atrial chamber can form — A is required regardless of D, C, and Φ.

Acute disruption of the fibrillar collagen network decreases myocardial systolic performance without changing myocyte contractility (Baicu et al., 2003). This is an example of the A-domain zero-term veto at the organ level in its purest form: the execution machinery (cardiomyocyte contractility,

© 2026 by the author(s). Distributed under a Creative Commons CC BY license.

Preprints.org (www.preprints.org) | NOT PEER-REVIEWED | Posted: 13 April 2026 doi:10.20944/preprints202604.0864.v1

electrochemical drive, triggering signals) is intact; the topological scaffold that couples that machinery to functional output has been disrupted; execution fails.

Wolff-Parkinson-White (WPW) syndrome provides a clinical demonstration of A-domain topology error producing pathological execution. Aberrant accessory atrioventricular conduction pathways are Bauplan topology errors — additional circuit connections that were not present in the normal topological template. The consequence is re-entrant tachyarrhythmias that are precisely predictable from the aberrant circuit geometry: D (electrochemical gradient), C (sinus node trigger), and Φ (action potential threshold) are intact; the wrong A-domain topology is present; a pathological execution program runs. This is another example of the zero-term veto inverted: a maladaptive A topology enables pathological execution rather than preventing it.

5.2. The Liver: Hepatostat, Lobular Topology, and Zonation

The liver strictly maintains its size at a predefined setpoint — the hepatostat — restoring the liver-to-body weight ratio to within a few percent following removal of two-thirds of hepatic mass within 7–10 days in rodents and approximately three months in humans (Michalopoulos and DeFrances, 1997; Fausto et al., 2012). What is the hepatostat actually targeting?

The hepatostat is not targeting cell number. It is targeting lobular topology: the hexagonal arrangement of hepatocytes around central veins, with portal triads at the six vertices, at a specific diffusion distance from sinusoids. This topology encodes two essential elements: (1) the Wnt gradient that runs from the pericentral zone (zone 3, high Wnt) to the periportal zone (zone 1, low Wnt), which specifies zone-specific metabolic gene expression; and (2) the bile acid flux that provides the C-domain signal for hepatostat termination. Zone 1 hepatocytes express gluconeogenesis and β-oxidation enzymes; zone 3 hepatocytes express glycolysis and lipid synthesis enzymes. This metabolic zonation is not determined by D or Φ — it is determined by positional identity within the lobular Bauplan.

The decellularization experiment settles the question of whether this A-domain topology is cell-encoded or scaffold-encoded. Complete removal of every cell from a human liver while preserving the ECM scaffold retains the lobular hexagonal topology: portal tracts remain in their characteristic positions, collagen I and III distribution is preserved in both sinusoids and portal tracts, and the three-dimensional sinusoidal network architecture survives decellularization (Mazza et al., 2015). Furthermore, hepatocytes reseeded onto a decellularized liver scaffold preferentially adopt zone-specific gene expression patterns consistent with their position relative to portal triads and central veins — the scaffold appears to encode positional identity (Huch et al., 2015). The Bauplan is etched into the permanent ECM scaffold.

Cirrhosis destroys this topology. Stellate cell activation and progressive collagen deposition replace the hexagonal lobular architecture with disorganized fibrous septa, obliterating the portal-central vein geometry and the Wnt gradient that depends on it. The consequence is loss of metabolic zonation despite abundant viable hepatocytes — $A \to 0$ from Bauplan destruction, producing hepatic execution failure that no plausible amount of hepatocyte proliferation (D), growth factor signaling (C), or YAP/TAZ permissiveness (Φ) can reverse, because the topological template that $D \times C \times \Phi$ would regenerate toward no longer exists.

5.3. The Kidney Nephron: Geometry as Mechanistic Prerequisite

The renal countercurrent multiplier system provides perhaps the most rigorous available demonstration that Bauplan topology is a mechanistic prerequisite for an execution event rather than merely a correlate of it. The loop of Henle concentrates urine by establishing a steep osmotic gradient in the renal medulla. This gradient depends absolutely on the hairpin geometry of the tubule: the descending limb must run parallel and antiparallel to the ascending limb over a specific length, so that the diluting action of the ascending limb (active NaCl reabsorption without water) amplifies the concentration in the descending limb and interstitium through countercurrent exchange.

© 2026 by the author(s). Distributed under a Creative Commons CC BY license.

Preprints.org (www.preprints.org) | NOT PEER-REVIEWED | Posted: 13 April 2026 doi:10.20944/preprints202604.0864.v1

Change the geometry — straighten the loop, shorten it, or alter the spatial relationship between descending and ascending limbs — and the countercurrent multiplication collapses regardless of how many transport proteins are expressed. The topology constitutes a primary mechanistic constraint. A perfectly functional set of ion transporters in a straight tubule would produce isotonic urine. This is an example of the Bauplan-as-A-domain argument in its most stringent form: the A-domain (loop geometry) is not merely required for the execution event (urine concentration)—it is the mechanistic implementation of that event. Without the Bauplan, the execution event is not degraded; it is physically impossible.

6. Empirical Proof Line 3: Minimal Systems

6.1. C. elegans: The Connectome as Literal Bauplan

The nematode *Caenorhabditis elegans* contains exactly 302 neurons with an invariant, completely mapped connectome — every cell division, every synapse, every position — established through serial electron microscopy (White et al., 1986). The connectome is the Bauplan in the most literal possible sense: it defines exactly which execution events are topologically possible, with a precision unmatched by any other biological system.

Laser ablation of specific identified neurons while leaving all others intact produces categorical behavioral loss that cannot be compensated by any other combination of D, C, and Φ. Ablation of the MC motor neuron abolishes pharyngeal pumping despite intact pharyngeal muscle (D intact), food-derived glutamate signals (C intact), and normal nematode metabolic state (Φ intact) — the A-domain zero-term veto from circuit Bauplan disruption, published and replicated across dozens of circuits (Avery and Horvitz, 1989). Ablation of the AVA interneurons abolishes backward locomotion; ablation of the HSN neurons abolishes egg-laying; ablation of the AWC chemosensory neurons abolishes attraction to volatile odorants. In each case, D, C, and Φ are present and cannot compensate for $A \rightarrow 0$.

The sterol link in C. elegans is direct: dafachronic acids, which are cholesterol-derived steroid hormones, regulate dauer entry — the developmental arrest state that represents one of the most dramatic threshold-governed biological decisions in any organism (Motola et al., 2006). The entire ARCH × Φ argument — Bauplan (A) as connectome, drive (D) as metabolic state, context (C) as population density and food availability, Φ as dafachronic acid-regulated nuclear hormone receptor gating — can be assembled from published C. elegans data in a single organism that unites the present paper's Bauplan argument with the companion paper's sterol-Φ argument.

6.2. Zebrafish: Vertebrate Escape Circuit Bauplan

The zebrafish Mauthner cell escape circuit is the most completely characterized vertebrate Bauplan for a single behavior: two giant neurons (one per side), invariant bilateral position in the hindbrain, invariant direct connectivity to spinal cord interneurons and trunk musculature, mediating the characteristic C-start escape response to sudden aversive stimuli. The morphogenesis and synaptogenesis of this circuit — including the stereotyped outgrowth of the lateral and ventral dendrites and the spatial distribution of identified afferent terminal classes — has been mapped at the level of individual identified synapses in developing zebrafish (Kimmel, Sessions, & Kimmel, 1981).

Mauthner cell ablation markedly impairs the C-start escape response despite intact trunk musculature, intact startle stimuli, and intact motivational state — a reduction in A from circuit Bauplan disruption that produces categorical behavioral failure not compensable by elevated sensory input or increased drive (Kimmel, Eaton, & Powell, 1980). When ablation is extended to include the giant axon as well as the soma, rapid escapes are lost permanently and this loss directly reduces survival in predator-prey assays, demonstrating that the survival-critical function depends specifically on this identified circuit element (Hecker et al., 2020). The transparency of zebrafish larvae allows simultaneous real-time imaging of circuit activity and behavioral output, providing direct

© 2026 by the author(s). Distributed under a Creative Commons CC BY license.

Preprints.org (www.preprints.org) | NOT PEER-REVIEWED | Posted: 13 April 2026 doi:10.20944/preprints202604.0864.v1

experimental access to A-domain Bauplan function unavailable in any other vertebrate (Kohashi & Oda, 2008).

Zebrafish sterol biosynthesis mutants extend this argument to the present paper's central claim. Mutations in post-squalene sterol biosynthetic enzymes produce both morphological Bauplan defects — skeletal dysplasia, craniofacial malformation, brain patterning errors — and behavioral deficits in the same animal, directly linking sterol availability to A-domain architecture during development and to Φ at the membrane level simultaneously (Mwinyi et al., 2020). Insufficient sterol can disrupt both the Bauplan-building role of cholesterol via Sonic hedgehog processing and the Φ-operating role via membrane dipole potential and ion channel gating.

6.3. Smith-Lemli-Opitz Syndrome: One Molecule, Two Roles

Smith-Lemli-Opitz (SLO) syndrome, caused by biallelic loss-of-function mutations in DHCR7 (7-dehydrocholesterol reductase), the final enzyme in cholesterol biosynthesis, produces simultaneous disruption of Bauplan construction and Φ modulation through the same molecular deficiency (Porter, 2008). The clinical phenotype is correspondingly simultaneous: digit abnormalities (polydactyly, 2-3 toe syndactyly), brain malformations (holoprosencephaly spectrum, corpus callosum agenesis), cardiac septal defects, and behavioral deficits including intellectual disability and autism-spectrum features.

The molecular mechanism bridges the two papers. Cholesterol is covalently attached to Sonic hedgehog protein during its autocatalytic processing — a cholesterol ester linkage that is required for proper membrane tethering, release as a morphogen, and long-range signaling activity (Porter et al., 1996). Without adequate cholesterol, Shh cannot be properly processed, the Bauplan-specifying gradient that determines digit identity and organ topology fails, and A-domain topology errors result. In parallel, inadequate cholesterol reduces membrane dipole potential, impairs lipid raft organization, and dysregulates ion channel kinetics — the direct membrane Φ mechanism of the companion paper. In SLO syndrome, a single enzymatic failure simultaneously degrades A (during development, through failed Shh-mediated Bauplan specification) and Φ (throughout life, through membrane composition effects on gating). The same molecule builds the gate and operates it.

7. The Four-Tier A-Domain Hierarchy: From Phylotypic to State

7.1. The Tier Structure

Not all A-domain constraints are equally permanent. We propose a four-tier hierarchy based on the timescale over which each tier is set and the degree to which it can be modified by downstream D, C, and Φ signals.

Table 1. Four-tier A-domain hierarchy. Only Tier IV is what ARCH × Φ gates in real time. Tiers I–III constitute the Bauplan — the upstream constraint that determines the ceiling of Tier IV execution.

Tier	Content	Set by	Timescale	Reversibility
I — Phylotypic	Body axis, organ topology, Hox patterning, ZRS-Shh circuit	Gastrulation and early organogenesis	Once per lifetime, irreversible	None on behavioral timescales
II — Ontogenetic	Adult size, organ proportions, allometry	Growth and metabolic rate	Developmental time	Limited; constrained by Tier I

© 2026 by the author(s). Distributed under a Creative Commons CC BY license.

Preprints.org (www.preprints.org) | NOT PEER-REVIEWED | Posted: 13 April 2026 doi:10.20944/preprints202604.0864.v1

III — Functional	ECM collagen topology, circuit wiring, receptor density	Development plus experience	Years; plastic	Partial; can be driven by Φ lock
IV — State	Posture, arousal, muscular pre-loading	Moment-to-moment signals	Seconds to minutes	Complete; what ARCH × Φ gates

Tiers I–III are effectively irreversible on behavioral timescales — they cannot be modified by any combination of D, C, and Φ to which a living organism has access. A snake that has lost its ZRS cannot regrow limbs regardless of Shh signaling. A cirrhotic liver cannot restore hexagonal lobular topology regardless of hepatocyte growth factor. An infarcted myocardium cannot reconstitute a sinus node from scar tissue regardless of electrical stimulation. These are not failures of D, C, or Φ — they are failures of A, the structural prerequisite above which all execution is negotiated.

7.2. YAP/TAZ Is Φ, Not A

A conceptual distinction that the existing Hippo/YAP-TAZ literature has not clearly drawn is between the organ-size regulator (which acts as Φ in the ARCH framework) and the organ-size template (which is A). YAP/TAZ nuclear permissiveness is Φ: it gates whether growth execution is permitted, responds to ECM mechanics (reading out A), and can be independently modulated by upstream signals including cell density, shear stress, and metabolic state (Piccolo et al., 2014). When YAP/TAZ is pharmacologically suppressed ($\Phi \to 0$), organ growth is arrested regardless of D and C (Hippo mutant overgrowth phenotypes demonstrate the Φ lock direction; verteporfin-mediated YAP/TAZ inhibition demonstrates the Φ veto direction).

YAP/TAZ is not A because it does not specify topological template. YAP/TAZ overactivation produces hepatic overgrowth (more cells, larger mass) without altering lobular hexagonal topology — the Wnt gradient is preserved, metabolic zonation persists, and the regeneration template remains intact (Camargo et al., 2007; Dong et al., 2007). This finding generalizes across size-control pathways: the Drosophila literature independently establishes that neither insulin/PI3K nor Hippo signaling alters organ topology when modulated in isolation, producing only metrical changes within a preserved patterning template (Hafen & Stocker, 2003; Yang & Xu, 2011). The consistent failure of size-control pathways to alter topological architecture across these systems is precisely what the ARCH framework predicts: Φ-domain manipulation moves the metrical output, not the topological ceiling. The organ has grown beyond its normal setpoint but retains its Bauplan. In the ARCH framework, this is Φ lock producing excess D × C × Φ-driven growth within an intact A-domain template — a metrical change, not a topological one. The set of topologically possible execution events has not changed; their frequency has increased.

Cirrhosis, by contrast, changes A: it destroys the lobular topology and eliminates the execution events (zone-specific metabolism, directed regeneration) that depend on it. YAP/TAZ is active in cirrhotic tissue, but it cannot drive regeneration toward the original lobular template because the scaffold that encodes that template is gone. Φ is permissive; A is destroyed; $R \to 0$. Therapies targeting Φ (YAP/TAZ inhibitors, neurosteroids, HDAC inhibitors) may be more effective when A is intact but Φ is locked; they will be insufficient when A itself has been destroyed.

© 2026 by the author(s). Distributed under a Creative Commons CC BY license.

Preprints.org (www.preprints.org) | NOT PEER-REVIEWED | Posted: 13 April 2026 doi:10.20944/preprints202604.0864.v1

8. Φ Lock Driving Tier III A Remodeling: Cardiac Hypertrophy and Fibrosis

8.1. Two Simultaneous Processes

Cardiac pressure overload initiates two distinct remodeling processes simultaneously, and their differential reversibility upon unloading is the key empirical demonstration of the Φ/A distinction at the organ level. The first process is chromatin-level gene program switching — the Brg1-HDAC-PARP ternary complex reactivation that drives the α-MHC to β-MHC isoform switch and the fetal gene program (Hang et al., 2010). This is Φ operating at the epigenetic tier, and it is pharmacologically reversible: HDAC inhibitors block the switch, attenuate hypertrophic growth in a dose-dependent fashion (Antos et al., 2003), and the histone modifications at the MHC loci normalize when the stress stimulus is withdrawn (Hang et al., 2010).

The second process is ECM collagen topology remodeling — sustained YAP/TAZ nuclear activity and fibroblast activation that produce progressive deposition of collagens I and III, cross-linking of immature collagen fibrils, and disorganization of the fibrillar collagen network (Weber et al., 1994; Travers et al., 2021). This is Tier III A remodeling — not a change in gene programs (Φ) but an alteration in the physical topology of the ECM scaffold that determines how mechanical forces propagate across cardiac tissue.

8.2. The LVAD Dissociation

Mechanical unloading by left ventricular assist device (LVAD) removes the hemodynamic D-domain signal and normalizes the YAP/TAZ Φ pathway. The cardiomyocyte-level Φ programs respond appropriately: myocyte diameter decreases by approximately 26% following sustained LVAD support, and the fetal gene program is substantially suppressed (Zafeiridis et al., 1998; Bruckner et al., 2001). These are Φ-level changes and they respond to Φ normalization. This cellular recovery is reflected at the organ level: LVAD support significantly improves LVEF, reduces chamber dimensions, and normalizes hemodynamic parameters in the majority of patients (Zafeiridis et al., 1998; Bruckner et al., 2001; Koshman et al., 2013; Saito et al., 2010).

The collagen topology does not respond. The degree of fibrosis at the time of LVAD implantation is itself a significant predictor of the magnitude of functional recovery — fibrosis burden at implantation correlates inversely with improvement in LVEF ($r = -0.637$, $p < 0.001$), LVEDD ($r = -0.725$), and LVESD ($r = -0.800$), and patients in whom the device was successfully explanted had significantly lower fibrosis than those who could not be weaned (Saito et al., 2010). Myocardial stiffness in control tissue is approximately 4 kPa; in pre-LVAD tissue it rises to approximately 11 kPa; and in post-LVAD tissue it remains at approximately 10 kPa — statistically elevated versus control despite months of effective hemodynamic unloading (Travers et al., 2021). Collagen content assessed by picrosirius red staining shows no significant reduction after LVAD support: 25.7% fibrosis area pre-LVAD versus 27.9% post-LVAD (Farris et al., 2017). The Tier III A change is maintained after the Φ signal that drove it has been removed.

The mechanism underlying this persistence identifies the irreversibility threshold precisely. Fibroblasts isolated from pre-LVAD and post-LVAD tissue, plated on substrates with stiffness reflecting either normal (~2 kPa) or fibrotic (~8 kPa) myocardium, show constitutive production of collagen α1(I) at similar levels on both substrates — unlike control fibroblasts, which produce collagen in a substrate-stiffness-dependent fashion (Travers et al., 2021). The mechano-sensing pathway that normally couples ECM stiffness to collagen production has been uncoupled. Post-LVAD fibroblasts can no longer read the mechanical signal that would tell them the scaffold is already stiff enough to stop producing collagen. They have undergone a cell-autonomous phenotypic conversion — a small-scale Bauplan change at the cell type level — that persists independently of the upstream hemodynamic signals that induced it. Figure 1 summarizes this discussion.

© 2026 by the author(s). Distributed under a Creative Commons CC BY license.

Preprints.org (www.preprints.org) | NOT PEER-REVIEWED | Posted: 13 April 2026 doi:10.20944/preprints202604.0864.v1

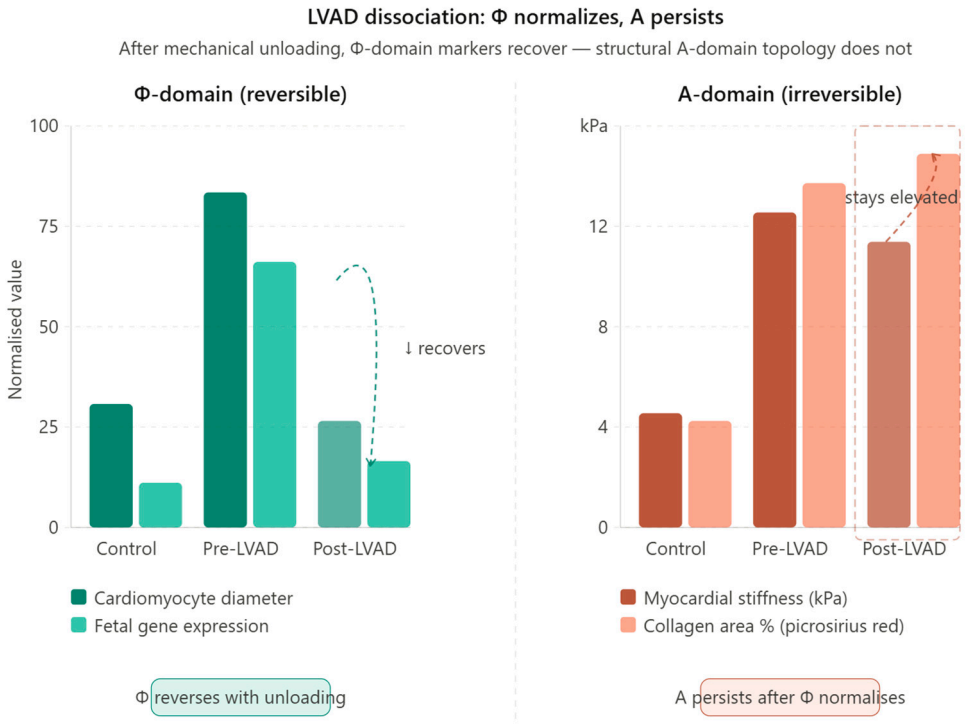

Figure 1. LVAD mechanical unloading dissociates Φ-domain recovery from A-domain persistence. Left panel: Φ-domain markers — cardiomyocyte diameter and fetal gene program expression — normalize substantially following LVAD support, consistent with reversal of pressure-overload signaling. Right panel: A-domain structural markers — myocardial passive stiffness (kPa) and collagen area fraction (picrosirius red) — remain elevated after equivalent unloading duration, statistically indistinguishable from pre-LVAD values. The dissociation demonstrates that Φ and A are independently regulated: normalization of the upstream hemodynamic signal restores gating-level programs while leaving ECM topology intact. Within the ARCH × Φ framework, this constitutes direct organ-level evidence that the A-domain is not downstream of Φ and cannot be restored by Φ modulation alone. Data from Zafeiridis et al. (1998), Farris et al., (2017), and Travers et al. (2021).

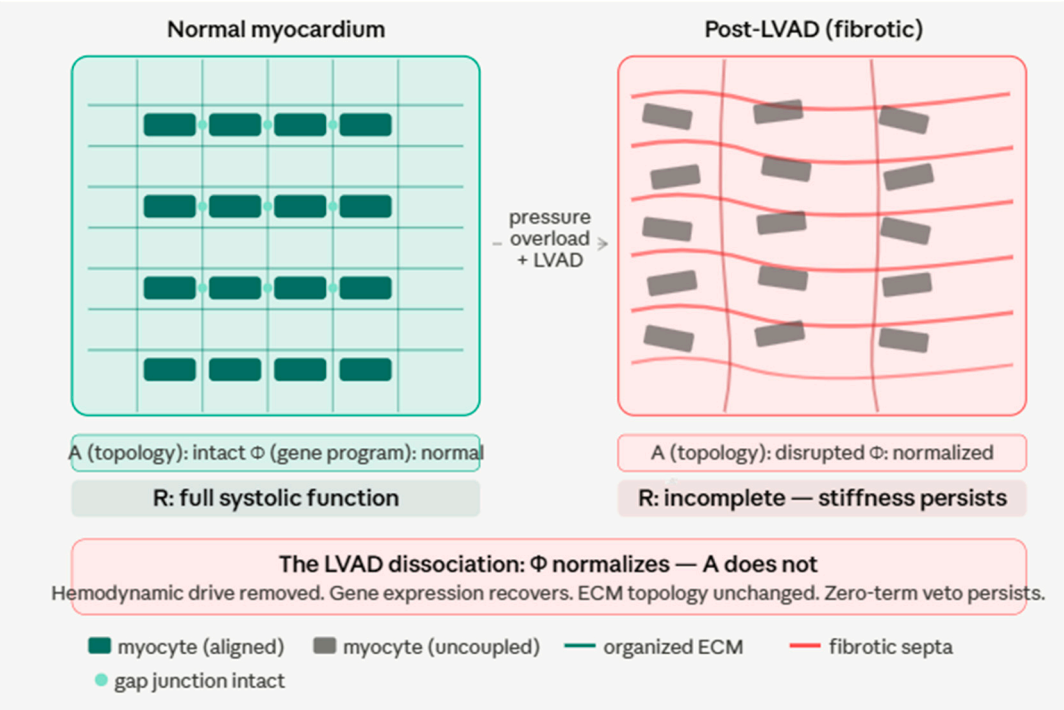

© 2026 by the author(s). Distributed under a Creative Commons CC BY license.

Preprints.org (www.preprints.org) | NOT PEER-REVIEWED | Posted: 13 April 2026 doi:10.20944/preprints202604.0864.v1

Figure 2. The LVAD dissociation: Φ normalizes, A does not. Normal myocardium (left) shows organized collagen scaffold, aligned cardiomyocytes, and intact intercalated disc coupling. Following pressure-overload fibrosis and LVAD unloading (right), hemodynamic drive is removed and gene expression normalizes — but ECM topology remains disrupted, cardiomyocytes are uncoupled, and Topological Connectivity Density (TCD) is unchanged. Within the ARCH × Φ framework ($R = A \times D \times C \times \Phi \geq \theta$), persistent A-domain disruption constitutes a zero-term veto on full recovery regardless of Φ normalization. Residual diastolic dysfunction after LVAD support is a predicted consequence of structural irreversibility.

8.3. The General Rule

This data instantiates the general rule for Tier III A remodeling: Φ can drive A upward into maladaptive attractors, but once collagen topology and fibroblast mechano-sensing cross a threshold, later Φ normalization cannot simply reverse the Bauplan change. The clinical consequence is reflected in the 3–5% LVAD explant rate — only 3–5% of patients achieve sufficient myocardial recovery for device removal (Birks et al., 2006). The cardiomyocyte-level Φ programs normalize; the heart cannot be explanted because the Tier III A topology that determines passive chamber mechanics has crossed the irreversibility boundary.

The ARCH framework frames the therapeutic implication precisely: interventions targeting Φ-level programs (HDAC inhibitors, YAP/TAZ modulators, neurosteroids) should be effective at preventing the transition and reversing early A remodeling when applied before the fibroblast mechano-sensing uncoupling occurs. Once established ECM collagen topology has crossed the irreversibility threshold, Φ-directed therapies are necessary but not sufficient — the Tier III A substrate must also be addressed through anti-fibrotic approaches that target the collagen network directly. The intervention window is definable: the period during which Φ is locked but A has not yet been remodeled beyond the mechano-sensing decoupling point.

9. Quantification: Topological Connectivity Density

9.1. The Problem

For the ARCH × Φ equation to be more than a theoretical framework, each term must in principle be measurable. Drive (D) can be estimated from portal pressure, wall stress, or metabolic demand. Context (C) can be operationalized from the magnitude of a specific trigger signal. Φ can be measured from YAP/TAZ nuclear-to-cytoplasmic ratio, passive myocardial stiffness, or histone acetylation state. The A-domain has presented the hardest measurement challenge: A is topological, not metrical.

Collagen volume fraction (CVF), measured from Masson trichrome or picrosirius red staining, is the current clinical standard for fibrosis assessment. CVF measures quantity but not topology. Cirrhosis and early fibrosis may have similar CVF values while representing dramatically different A-domain states — the early fibrotic liver retains hexagonal lobular topology while the cirrhotic liver has replaced it with fibrous nodules. A metric that distinguishes these two states is required. The morphometrics literature has long formalized an analogous distinction at the population level: geometric morphometrics characterizes the spatial configuration of homologous landmarks independent of size, providing topological information that allometric scaling coefficients cannot capture (Cobham & Mirth, 2020). TCD extends this logic from surface landmark geometry to three-dimensional ECM fiber network topology, making it applicable to biopsy sections rather than whole-organ surface reconstructions, and operationalizing the A-domain state within the ARCH equation rather than serving as a descriptive population statistic.

9.2. Fractal Dimension and TCD

The fractal dimension of the collagen fiber network provides a candidate measure of topological information. Fractal dimension measures the spatial complexity of a network — a densely branching, isotropic network characteristic of organized lobular collagen has a different fractal dimension than

© 2026 by the author(s). Distributed under a Creative Commons CC BY license.

Preprints.org (www.preprints.org) | NOT PEER-REVIEWED | Posted: 13 April 2026 doi:10.20944/preprints202604.0864.v1

an equivalent mass of parallel collagen bundles or random fibrous septa. In pulmonary fibrosis, fractal dimension increases with fibrosis progression while providing information about collagen network reorganization that is independent of collagen content — detectable even when conventional collagen quantification shows no change (Casey et al., 2024; Hall et al., 2025). In intestinal fibrosis in Crohn's disease, fractal dimension of the extracellular matrix provides observer-independent quantification that correlates significantly with histological fibrosis scores and outperforms semiquantitative scoring systems (Weber et al., 2024).

Second harmonic generation (SHG) microscopy is the imaging modality that makes topological A-domain quantification clinically tractable. SHG is label-free, generates quantitative images of fibrillar collagen topology from standard biopsy sections, and is compatible with automated digital image analysis and machine learning scoring (Campagnola & Loew, 2003; Eftimie et al., 2024). SHG combined with AI analysis has been used to quantify 184 distinct fibrosis parameters across various regions of the liver lobule, and to differentiate progressive versus regressive septal fibrosis in cirrhosis (Naoumov et al., 2022).

We define Topological Connectivity Density (TCD) as:

$$TCD(R) = D\_f(R) \times \kappa(R)/\kappa\_ref$$

where D_f(R) is the fractal dimension of the collagen fiber network in tissue region R computed from SHG images, κ(R) is the mean node degree of the skeletonized fiber network (capturing branching topology at fiber intersections), and κ_ref is the organ-specific and species-specific reference value for healthy tissue. The dimensionless quotient κ(R)/κ_ref normalizes the branching topology measure to the healthy Bauplan reference, yielding TCD ≈ 1 for normal tissue and TCD → 0 as Bauplan topology is destroyed.

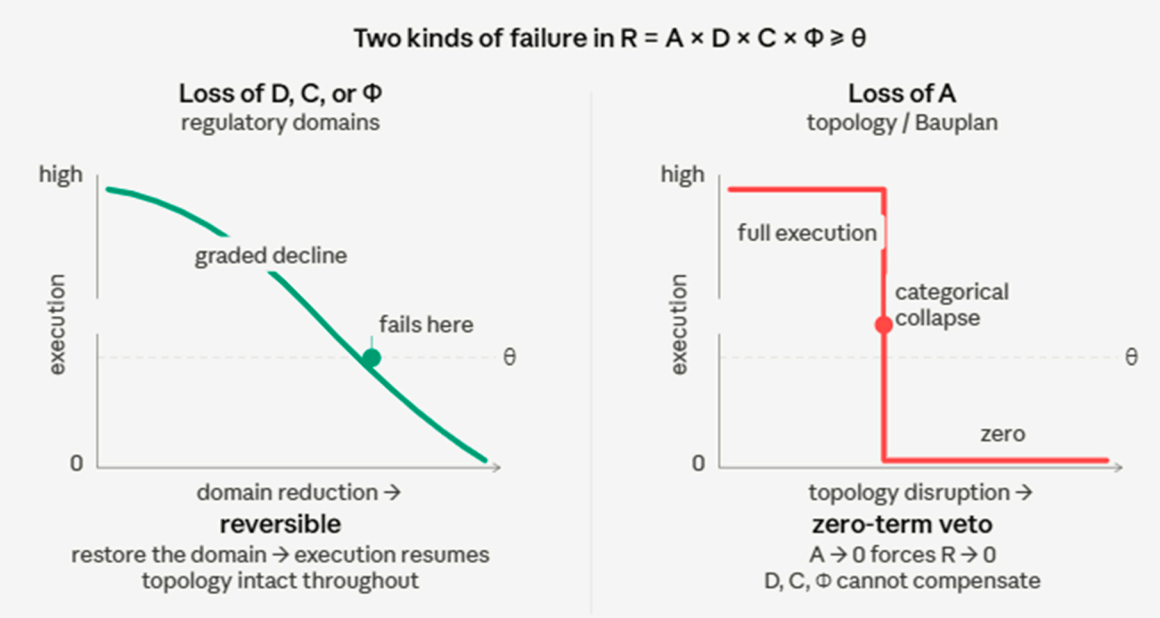

9.3. Validation and Properties

Three properties distinguish TCD from existing fibrosis metrics and support its use as an A-domain operationalization. First, TCD is topology-sensitive rather than quantity-sensitive. Cirrhotic liver has massively increased CVF but destroyed lobular topology; TCD falls because node connectivity is low (fibrous septa have few branching nodes compared to the sinusoidal network) and spatial autocorrelation across the lobular unit is disrupted, even though D_f may remain elevated. CVF rises; TCD falls; only TCD captures the A-domain state.

© 2026 by the author(s). Distributed under a Creative Commons CC BY license.

Preprints.org (www.preprints.org) | NOT PEER-REVIEWED | Posted: 13 April 2026 doi:10.20944/preprints202604.0864.v1

Second, the decellularization literature provides independent experimental validation. A decellularized normal liver scaffold retains a TCD value close to TCD_ref because the collagen fiber network topology is preserved (Mazza et al., 2015; Baptista et al., 2011). An identically processed cirrhotic liver retains similar collagen volume but dramatically reduced TCD because the topological connectivity has been destroyed. The decellularized normal liver can support hepatocyte reseeding and reconstitute metabolic zonation; the decellularized cirrhotic liver cannot (Huch et al., 2015). TCD might predict which scaffold can support A-domain regeneration.

Third, TCD defines a reference setpoint (TCD_ref) that can be organ-specific, disease-specific, and species-specific, established from healthy tissue. The normalized TCD(t) ∈ [0,1] provides the dimensionless A value that enters the ARCH equation. The commitment threshold θ for execution failure is empirically determined as the critical TCD value below which execution fails categorically — predicted by the Φ-reversibility principle to vary systematically with the cost of irreversible A-domain commitment errors across organ systems.

10. Disease Failure Modes and Falsifiable Predictions

10.1. Three Failure Modes

Table 2. Three A-domain failure modes distinguished by mechanism, clinical instantiation, and predicted response to Φ-directed therapy. DCM: dilated cardiomyopathy; MS: multiple sclerosis; SLO: Smith-Lemli-Opitz syndrome.

Failure Mode	Mechanism	Clinical Example	ARCH Prediction	Φ-Therapy Expected Effective?
A → 0 (congenital)	Bauplan topology never formed; ZRS/Hox/ECM morphogen disruption	Congenital heart defects (ISL1 mutation); polydactyly (ZRS mutation); SLO syndrome	Categorical execution failure irreversible by D, C, or Φ manipulation	No — A must be rebuilt; not addressable by Φ modulation
A erosion (acquired)	Progressive Bauplan destruction; cirrhosis, DCM, MS plaques	Cirrhosis → metabolic zonation loss; DCM → systolic failure; MS → conduction block	Execution failure proportional to A erosion; no compensation threshold	Only if A template survives; ineffective once template destroyed
Φ lock → A remodeling	Sustained Φ-active state drives Tier III ECM remodeling beyond reversibility threshold	Pathological cardiac hypertrophy → fibrosis; pressure-overload DCM	Partial irreversibility; Φ-tier reversal possible but collagen topology persists	Effective if applied before fibroblast mechano-sensing uncoupling; insufficient after

10.2. Falsifiable Predictions

The framework generates six predictions that are independent of the prior instantiations and testable with existing technology.

Prediction 1 (Snake ZRS resurrection). Restoring a fully functional ZRS into the python genome should not restore functional hindlimbs, because downstream Hox regulatory sequences and structural limb-development genes have also degraded following ZRS loss (Kvon et al., 2016). A-

© 2026 by the author(s). Distributed under a Creative Commons CC BY license.

Preprints.org (www.preprints.org) | NOT PEER-REVIEWED | Posted: 13 April 2026 doi:10.20944/preprints202604.0864.v1

domain specification is multi-component; single-enhancer rescue is insufficient once multiple Bauplan components have eroded. This tests the multi-component nature of A.

Prediction 2 (Hepatostat topology vs. mass). In partial hepatectomy models, preventing lobular topology reconstitution (by integrin-linked kinase knockout or portal hypertension manipulation) while allowing cell mass restoration should produce metabolic zonation failure independent of total hepatocyte number. This distinguishes A-domain (topology) from D-domain (mass/demand) accounts of the hepatostat.

Prediction 3 (Hapln1a rescue). In zebrafish hapln1a mutants, restoring atrial volume by mechanical stretch while bypassing ECM-mediated morphogen gradient reconstitution should produce conduction geometry errors — A-domain topology errors from bypassing Bauplan specification. This tests whether A is ECM topology or merely the cell count it produces.

Prediction 4 (SLO sterol timing). In SLO animal models, embryonic cholesterol supplementation during the Shh-dependent patterning window should rescue Bauplan topology (A) more effectively than postnatal supplementation, which restores membrane Φ but cannot reverse already-specified developmental programs. This distinguishes the A-building role of cholesterol (developmental, irreversible once patterning completes) from the Φ-operating role (continuous, reversible).

Prediction 5 (TCD as a predictor of regenerative capacity). In liver transplantation from donors with varying degrees of fibrosis, TCD computed from donor biopsy sections should predict post-transplant metabolic function more accurately than CVF alone, because TCD captures whether the A-domain template for zonation is intact.

Prediction 6 (LVAD timing window). LVAD implantation accompanied by anti-fibrotic therapy (HDAC inhibitor or direct collagen crosslink inhibitor) applied within the first weeks of pressure overload should achieve higher myocardial recovery rates than LVAD alone, because the combined therapy prevents the fibroblast mechano-sensing uncoupling that produces Tier III A irreversibility.

The Bauplan-as-A proposal is explicitly testable. First, the framework predicts that Topological Connectivity Density (TCD), quantified from second-harmonic generation images of standard biopsies, will track irreversible Tier III A-domain remodeling more faithfully than bulk fibrosis measures (for example, collagen proportionate area) across cirrhosis and dilated cardiomyopathy cohorts matched for conventional staging. Second, in prospective studies of ventricular reverse remodeling after left ventricular assist device placement or intensive guideline-directed medical therapy, pre-treatment TCD should cap the ceiling of functional recovery even when D, C, and Φ are favorably manipulated. Third, organoids or engineered tissues grown on scaffolds with identical cell types and growth-factor environments but systematically altered ECM topology should show execution phenotypes (e.g., conduction, countercurrent multiplication, zonation) that follow scaffold topology rather than cell-intrinsic or soluble-factor manipulations. Together, these experiments would discriminate the Bauplan-as-A hypothesis from models in which organ-level execution is governed primarily by metrical growth control or cell-autonomous signaling.

11. Conclusion

The ARCH × Φ framework describes biological execution as a multiplicative threshold event requiring the conjunctive alignment of Archetype, Drive, Context, and Gating Field. The present paper proposes that the Archetype — the conserved structural prerequisite for execution — has internal hierarchical structure, and that this structure is the Bauplan: the conserved topological architecture of organs and appendages that is encoded in cis-regulatory elements, ECM scaffolds, and circuit wiring, set during morphogenesis, and etched permanently into the physical substrate of the organism.

Four lines of empirical evidence converge on this claim. The fin-to-limb appendage system demonstrates that a 770 bp cis-regulatory element conserved across 400 million years of vertebrate evolution encodes the topological A-domain specification for the appendage, that this specification functionally transfers across species, that it predates the structures it specifies, and that its progressive

© 2026 by the author(s). Distributed under a Creative Commons CC BY license.

Preprints.org (www.preprints.org) | NOT PEER-REVIEWED | Posted: 13 April 2026 doi:10.20944/preprints202604.0864.v1

erosion in snakes produces categorical execution failure in precise proportion to the degree of Bauplan degradation. Organ topology demonstrates that ECM scaffold disruption leads to execution failure independent of cellular viability, that the liver's topological setpoint is etched into the ECM scaffold rather than the cells, and that conduction system topology errors produce pathological execution with mathematical precision. Minimal model systems in C. elegans and zebrafish demonstrate the zero-term veto effect of Bauplan ablation, with the specificity of identified cells. Pathological cardiac hypertrophy demonstrates that sustained Φ lock can drive Tier III A remodeling beyond the reversibility threshold, producing partial irreversibility that cannot be fully addressed by Φ-directed therapy alone.

Sterols connect both papers: the same molecular class that contributes to Bauplan formation during development — through cholesterol-dependent Sonic hedgehog processing and signaling — also operates the gating mechanism throughout life via membrane Φ, neurosteroid Φ, and, potentially, epigenetic Φ through oxysterol–DNMT1 and steroid hormone–nuclear receptor–chromatin remodeling pathways. The same molecular class that contributed to early biological structure may continue to influence which configurations are permitted to be executed. These observations suggest a dual role — building and gating — operating across evolutionary and physiological timescales.

Disclosures

AI Use: The author used AI-assisted writing tools (Claude, Anthropic) during the preparation of this manuscript for language editing and structural feedback. The author takes full responsibility for the scientific content, accuracy of citations, and all intellectual contributions presented herein.

The author declares no competing interests.

No new data were generated or analyzed in this study.

References

Antos CL, McKinsey TA, Dreitz M, Hollingsworth LM, Zhang CL, Schreiber K, et al. Dose-dependent blockade to cardiomyocyte hypertrophy by histone deacetylase inhibitors. J Biol Chem. 2003;278(31):28930-7. doi:10.1074/jbc.M303113200

Avery L, Horvitz HR. Pharyngeal pumping continues after laser killing of the pharyngeal nervous system of C. elegans. Neuron. 1989;3(4):473-85. doi:10.1016/0896-6273(89)90206-7

Baicu CF, Stroud JD, Livesay VA, Hapke E, Holder J, Spinale FG, et al. Changes in extracellular collagen matrix alter myocardial systolic performance. Am J Physiol Heart Circ Physiol. 2003;284(1):H122-32. doi:10.1152/ajpheart.00233.2002

Baptista PM, Siddiqui MM, Lozier G, Rodriguez SR, Atala A, Soker S. The use of whole organ decellularization for the generation of a vascularized liver organoid. Hepatology. 2011;53(2):604-17. doi:10.1002/hep.24067

Barr AR, Heldt FS, Zhang T, Bakal C, Novak B. A dynamical framework for the all-or-none G1/S transition. Cell Syst. 2016;2(1):27-37. doi:10.1016/j.cels.2016.01.001

Bell SP, Dutta A. DNA replication in eukaryotic cells. Annu Rev Biochem. 2002;71:333-74. doi:10.1146/annurev.biochem.71.110601.135425

Birks EJ, Tansley PD, Hardy J, George RS, Bowles CT, Burke M, et al. Left ventricular assist device and drug therapy for the reversal of heart failure. N Engl J Med. 2006;355(18):1873-84. doi:10.1056/NEJMoa053063

Böhm J, Scherzer S, Krol E, Kreuzer I, von Meyer K, Lorey C, et al. The Venus flytrap Dionaea muscipula counts prey-induced action potentials to induce sodium uptake. Curr Biol. 2016;26(3):286-95. doi:10.1016/j.cub.2015.11.057

Bruckner BA, Stetson SJ, Perez-Verdia A, Youker KA, Radovancevic B, Connelly JH, et al. Regression of fibrosis and hypertrophy in failing myocardium following mechanical circulatory support. J Heart Lung Transplant. 2001;20(4):457-64. doi:10.1016/S1053-2498(00)00321-1

Camargo FD, Gokhale S, Johnnidis JB, Fu D, Bell GW, Jaenisch R, et al. YAP1 increases organ size and expands undifferentiated progenitor cells. Curr Biol. 2007;17(23):2054-60. doi:10.1016/j.cub.2007.10.039

© 2026 by the author(s). Distributed under a Creative Commons CC BY license.

Preprints.org (www.preprints.org) | NOT PEER-REVIEWED | Posted: 13 April 2026 doi:10.20944/preprints202604.0864.v1

Campagnola PJ, Loew LM. Second-harmonic imaging microscopy for visualizing biomolecular arrays in cells, tissues and organisms. Nat Biotechnol. 2003;21(11):1356-60. doi:10.1038/nbt894

Casas L, Saborido-Rey F, Ryu T, Michell C, Ravasi T, Irigoien X. Sex change in clownfish: molecular insights from transcriptome analysis. Sci Rep. 2016;6:35461. doi:10.1038/srep35461

Casey DT, Lahue KG, Mori V, Herrmann J, Hall JK, Suki B, et al. Local fractal dimension of collagen detects increased spatial complexity in fibrosis. Histochem Cell Biol. 2024;161(1):29-42. doi:10.1007/s00418-023-02238-4

Christoffels VM, Moorman AF. Development of the cardiac conduction system: why are some regions of the heart more arrhythmogenic than others? Circ Arrhythm Electrophysiol. 2009;2(2):195-207. doi:10.1161/CIRCEP.108.829341

Cobham AE, Mirth CK. The development of body and organ shape. BMC Zool. 2020;5:14. doi:10.1186/s40850-020-00063-5

Davis MC, Dahn RD, Shubin NH. An autopodial-like pattern of Hox expression in the fins of a basal actinopterygian fish. Nature. 2007;447(7143):473-6. doi:10.1038/nature05838

Derrick CJ, Sanchez-Posada J, Hussein F, Tessadori F, Pollitt EJ, Savage AM, et al. Asymmetric Hapln1a drives regionalized cardiac ECM expansion and promotes heart morphogenesis in zebrafish development. Cardiovasc Res. 2022;118(1):226-40. doi:10.1093/cvr/cvab004

Dong J, Feldmann G, Huang J, Wu S, Zhang N, Comerford SA, et al. Elucidation of a universal size-control mechanism in Drosophila and mammals. Cell. 2007;130(6):1120-33. doi:10.1016/j.cell.2007.07.019

Eftimie LG, Padrez Y, Golubewa L, Rutkauskas D, Hristu R. Widefield polarization-resolved second harmonic generation imaging of entire thyroid nodule sections for the detection of capsular invasion. Biomed Opt Express. 2024;15(8):4705-18. doi:10.1364/BOE.528788

Farris SD, Don C, Helterline D, Costa C, Plummer T, Steffes S, Mahr C, Mokadam NA, Stempien-Otero A. Cell-Specific Pathways Supporting Persistent Fibrosis in Heart Failure J Am Coll Cardiol. 2017 Jul 18;70(3):344–354. doi: 10.1016/j.jacc.2017.05.040.

Fausto N, Campbell JS, Riehle KJ. Liver regeneration. J Hepatol. 2012;57(3):692-4. doi:10.1016/j.jhep.2012.04.016

Gilham D, Wasiak S, Daze E, Boulet L, Laliberte S, Chami M, et al. BET inhibition reduces hepatic steatosis and liver fibrosis through a BET-bromodomain- and cholesterol-dependent mechanism in HFD-fed mice. Eur J Pharmacol. 2022;924:174964. doi:10.1016/j.ejphar.2022.174964

Hafen E, Stocker H. How are the sizes of cells, organs, and bodies controlled? PLoS Biol. 2003;1(3):e86. doi:10.1371/journal.pbio.0000086

Hall JK, Mori V, Herrmann J, Casey DT, Suki B, Bates JH, et al. Imaging the extracellular matrix structure and remodeling in healthy, fibrotic, and emphysematous human precision-cut lung slices. Respir Res. 2025;26. doi:10.1186/s12931-025-03464-7

Hang CT, Yang J, Han P, Cheng HL, Shang C, Ashley E, et al. Chromatin regulation by Brg1 underlies heart muscle development and disease. Nature. 2010;466(7302):62-7. doi:10.1038/nature09130

Hedrich R, Salvador-Recatala V, Dreyer I. Electrical wiring and long-distance plant communication. Trends Plant Sci. 2016;21(5):376-87. doi:10.1016/j.tplants.2016.01.016

Hecker A, Schulze W, Oster J, Richter DO, Schuster S. Removing a single neuron in a vertebrate brain forever abolishes an essential behavior. Proc Natl Acad Sci USA. 2020;117(6):3254-60. doi:10.1073/pnas.1820896117

Huch M, Gehart H, van Boxtel R, Hamer K, Blokzijl F, Verstegen MM, et al. Long-term culture of genome-stable bipotent stem cells from adult human liver. Cell. 2015;160(1-2):299-312. doi:10.1016/j.cell.2014.11.050

Jiang QX. Cholesterol-dependent gating effects on ion channels. Adv Exp Med Biol. 2019;1115:167-90. doi:10.1007/978-3-030-04278-3_8

Kee HJ, Sohn IS, Nam KI, Park JE, Qian YR, Yin Z, et al. Inhibition of histone deacetylation blocks cardiac hypertrophy induced by angiotensin II infusion and aortic banding. Circulation. 2006;113(1):51-9. doi:10.1161/CIRCULATIONAHA.105.559724

Kemper JK, Xiao Z, Ponugoti B, Miao J, Fang S, Kanamaluru D, et al. FXR acetylation is normally dynamically regulated by p300 and SIRT1 but constitutively elevated in metabolic disease states. Cell Metab. 2009;10(5):392-404. doi:10.1016/j.cmet.2009.09.009

© 2026 by the author(s). Distributed under a Creative Commons CC BY license.

Preprints.org (www.preprints.org) | NOT PEER-REVIEWED | Posted: 13 April 2026 doi:10.20944/preprints202604.0864.v1

Kimmel CB, Sessions SK, Kimmel RJ. Morphogenesis and synaptogenesis of the zebrafish Mauthner neuron. J Comp Neurol. 1981;198(1):101-20. doi:10.1002/cne.901980110

Kimmel CB, Eaton RC, Powell SL. Decreased fast-start performance of zebrafish larvae lacking Mauthner neurons. J Comp Physiol. 1980;140:343-50. doi:10.1007/BF00606073

Kohashi T, Oda Y. Initiation of Mauthner- or non-Mauthner-mediated fast escape evoked by different modes of sensory input. J Neurosci. 2008;28(42):10641-53. doi:10.1523/JNEUROSCI.1435-08.2008

Koshman YE, Patel N, Chu M, Iyengar R, Kim T, Ersahin C, Lewis W, Heroux A, Samarel AM. Regulation of connective tissue growth factor gene expression and fibrosis in human heart failure. J Card Fail. 2013 Apr;19(4):283-94. doi: 10.1016/j.cardfail.2013.01.013.

Kvon EZ, Kamneva OK, Melo US, Barozzi I, Osterwalder M, Mannion BJ, et al. Progressive loss of function in a limb enhancer during snake evolution. Cell. 2016;167(3):633-642.e11. doi:10.1016/j.cell.2016.09.028

Leal F, Cohn MJ. Loss and re-emergence of legs in snakes by modular evolution of Sonic hedgehog and HOXD enhancers. Curr Biol. 2016;26(21):2966-73. doi:10.1016/j.cub.2016.09.020

Lettice LA, Heaney SJ, Purdie LA, Li L, de Beer P, Oostra BA, et al. A long-range Shh enhancer regulates expression in the developing limb and fin and is associated with preaxial polydactyly. Hum Mol Genet. 2003;12(14):1725-35. doi:10.1093/hmg/ddg180

Lettice LA, Hill AE, Devenney PS, Hill RE. Point mutations in a distant Sonic hedgehog cis-regulator generate a variable regulatory output responsible for preaxial polydactyly. Hum Mol Genet. 2008;17(7):978-85. doi:10.1093/hmg/ddm370

Lettice LA, Devenney P, De Angelis C, Hill RE. The conserved Sonic hedgehog limb enhancer consists of discrete functional elements that regulate precise spatial expression. Cell Rep. 2017;20(6):1396-408. doi:10.1016/j.celrep.2017.07.037

Mazza G, Rombouts K, Hall AR, Urbani L, Luong TV, Al-Akkad W, et al. Decellularized human liver as a natural 3D-scaffold for liver bioengineering and transplantation. Sci Rep. 2015;5:13079. doi:10.1038/srep13079

Meaney S. Epigenetic regulation of cholesterol homeostasis. Front Genet. 2014;5:311. doi:10.3389/fgene.2014.00311

Michalopoulos GK, DeFrances MC. Liver regeneration. Science. 1997;276(5309):60-6. doi:10.1126/science.276.5309.60

Miyaoka Y, Ebato K, Kato H, Arakawa S, Shimizu S, Miyajima A. Hypertrophy and unconventional cell division of hepatocytes underlie liver regeneration. Curr Biol. 2012;22(13):1166-75. doi:10.1016/j.cub.2012.05.016

Motola DL, Cummins CL, Rottiers V, Sharma KK, Li T, Li Y, et al. Identification of ligands for DAF-12 that govern dauer formation and reproduction in C. elegans. Cell. 2006;124(6):1209-23. doi:10.1016/j.cell.2006.01.037

Mwinyi J, Lindberg J, Hamsten A, Hellenius ML, Lagercrantz J, Orho-Melander M, et al. Zebrafish models of skeletal dysplasia induced by cholesterol biosynthesis deficiency. Dis Model Mech. 2020;13(6):dmm042549. doi:10.1242/dmm.042549

Naoumov NV, Brees D, Locker J, et al. Digital pathology with artificial intelligence analyses provides greater insights into treatment-induced fibrosis regression in NASH. J Hepatol. 2022;77(5):1399-409. doi:10.1016/j.jhep.2022.06.018

Parker CG, Gruenhagen GW, Hegarty BE, Histed AR, Streelman JT, Rhodes JS, et al. Adult sex change leads to extensive forebrain reorganization in clownfish. Biol Sex Differ. 2024;15(1):58. doi:10.1186/s13293-024-00632-0

Parker CG, Lee JS, Histed AR, Craig SE, Rhodes JS. Stable and persistent male-like behavior during male-to-female sex change in the common clownfish Amphiprion ocellaris. Horm Behav. 2022;145:105239. doi:10.1016/j.yhbeh.2022.105239

Piccolo S, Dupont S, Cordenonsi M. The biology of YAP/TAZ: Hippo signaling and beyond. Physiol Rev. 2014;94(4):1287-312. doi:10.1152/physrev.00005.2014

Porter FD. Smith-Lemli-Opitz syndrome: pathogenesis, diagnosis and management. Eur J Hum Genet. 2008;16(5):535-41. doi:10.1038/ejhg.2008.10

Porter JA, Young KE, Beachy PA. Cholesterol modification of hedgehog signaling proteins in animal development. Science. 1996;274(5285):255-9. doi:10.1126/science.274.5285.255

© 2026 by the author(s). Distributed under a Creative Commons CC BY license.

Preprints.org (www.preprints.org) | NOT PEER-REVIEWED | Posted: 13 April 2026 doi:10.20944/preprints202604.0864.v1

Rahman T, Zorumski CF, Meloy JR. The ARCH model: a neuroevolutionary framework for behavioral execution. Front Psychiatry. 2025;16:1669530. doi:10.3389/fpsyt.2025.1669530

Rahman T. A multiplicative behavioral model of DNA replication initiation in cells. Open Life Sci. 2025;20(1):20251229. doi:10.1515/biol-2025-1229

Rahman T. Sex change in clownfish as an ARCH-governed biological decision. Horm Behav. 2026;180:105907. doi:10.1016/j.yhbeh.2026.105907

Rahman T. Threshold decision-making in the Venus flytrap. Plant Sci. 2026;365:113010. doi:10.1016/j.plantsci.2026.113010

Sagai T, Hosoya M, Mizushina Y, Tamura M, Shiroishi T. Elimination of a long-range cis-regulatory module causes complete loss of limb-specific Shh expression and truncation of the mouse limb. Development. 2005;132(4):797-803. doi:10.1242/dev.01613

Saito S, Matsumiya G, Sakaguchi T, Miyagawa S, Yamauchi T, Kuratani T, et al. Cardiac fibrosis and cellular hypertrophy decrease the degree of reverse remodeling and improvement in cardiac function during left ventricular assist device support. J Heart Lung Transplant. 2010;29:672-9. doi:10.1016/j.healun.2009.12.011

Shubin N, Tabin C, Carroll S. Deep homology and the origins of evolutionary novelty. Nature. 2009;457(7231):818-23. doi:10.1038/nature07891

Sun W, Luo Y, Lee AM, Bhargava A, Sato M, Bhate S, et al. Nonlinear optical microscopy: use of second harmonic generation and two-photon microscopy for automated quantitative liver fibrosis studies. J Biomed Opt. 2008;13(6):064010. doi:10.1117/1.3041159

Travers JG, Wennersten SA, Pena B, Bagchi RA, Smith HE, Hirsch RA, et al. HDAC inhibition reverses preexisting diastolic dysfunction and blocks covert extracellular matrix remodeling. Circulation. 2021;143(19):1874-90. doi:10.1161/CIRCULATIONAHA.120.046462

Wang Y, Chen L, Pandak WM, Heuman D, Hylemon PB, Ren S. High glucose induces lipid accumulation via 25-hydroxycholesterol DNA-CpG methylation. iScience. 2020;23(5):101102. doi:10.1016/j.isci.2020.101102

Weber MC, Schmidt K, Buck A, Kasajima A, Becker S, Li C, et al. Fractal analysis of extracellular matrix for observer-independent quantification of intestinal fibrosis in Crohn's disease. Sci Rep. 2024;14(1):3988. doi:10.1038/s41598-024-54545-4

Weber KT, Sun Y, Katwa LC. Myofibroblasts and local angiotensin II in rat cardiac tissue repair. Int J Biochem Cell Biol. 1994;26(3):323-42. doi:10.1016/S1357-2725(96)00116-1

Weatherbee SD, Halder G, Kim J, Hudson A, Carroll S. Ultrabithorax regulates genes at several levels of the wing-patterning hierarchy to shape the development of the Drosophila haltere. Genes Dev. 1998;12(10):1474-82. doi:10.1101/gad.12.10.1474

White JG, Southgate E, Thomson JN, Brenner S. The structure of the nervous system of the nematode Caenorhabditis elegans. Philos Trans R Soc Lond B Biol Sci. 1986;314(1165):1-340. doi:10.1098/rstb.1986.0056

Yang X, Xu T. Molecular mechanism of size control in development and human diseases. Cell Res. 2011;21(5):715-29. doi:10.1038/cr.2011.63

Zanconato F, Cordenonsi M, Piccolo S. YAP/TAZ at the roots of cancer. Cancer Cell. 2016;29(6):783-803. doi:10.1016/j.ccell.2016.05.005

Zafeiridis A, Jeevanandam V, Houser SR, Margulies KB. Regression of cellular hypertrophy after left ventricular assist device support. Circulation. 1998;98(7):656-62. doi:10.1161/01.CIR.98.7.656

Disclaimer/Publisher's Note: The statements, opinions and data contained in all publications are solely those of the individual author(s) and contributor(s) and not of MDPI and/or the editor(s). MDPI and/or the editor(s) disclaim responsibility for any injury to people or property resulting from any ideas, methods, instructions or products referred to in the content.

© 2026 by the author(s). Distributed under a Creative Commons CC BY license.